

Propagation characteristics of extratropical planetary waves observed in the ATSR global sea surface temperature record

Katherine L. Hill¹ and Ian S. Robinson

School of Ocean and Earth Science, Southampton Oceanography Centre, Southampton, England, United Kingdom

Paolo Cipollini

James Rennell Division for Ocean Circulation and Climate, Southampton Oceanography Centre, Southampton, England, United Kingdom

Abstract. This paper examines the characteristics of planetary wave signatures that have been found in the Along Track Scanning Radiometer averaged sea surface temperature (ASST) record for 1991-1996. Longitude-time plots for every latitude between 5° and 50°, north and south, reveal westward propagating wave-like patterns at many locations, whose speed decreases with latitude like baroclinic Rossby waves. A two-dimensional Radon transform method is used to measure the wave speed and its variation with location and time, which broadly matches the Rossby wave speeds predicted by the most recent theory and those measured by TOPEX altimetry, although there are some discrepancies. At low latitudes the thermally detected speeds are slower than expected, a possible consequence of sampling limitations. Wave signatures are clearest between 25° and 40°S, where the meridional temperature gradient is strongest. Here observed speeds are 20-30% greater than theoretical predictions. Planetary wave speed varies considerably with longitude. In general, it increases toward the west of ocean basins, and distinct differences between ocean basins are evident. The propagation characteristics of the waves appear to change abruptly at locations consistent with latitudinal variations in seafloor bathymetry, particularly midocean ridges. In addition, eastward propagating signatures are found in the Southern Ocean. The results demonstrate the value of the ASST data set as a tool for studying basin-scale wave processes as a complement to the use of altimetry. By observing the thermal signature of Rossby waves the method has the potential to clarify their influence on air-sea interaction processes and to contribute to climate modeling studies.

1. Introduction

This paper examines the sea surface thermal signatures of planetary waves in the ocean and measures their propagation speed. It is particularly concerned with detecting slowly moving thermal anomalies that have the propagation characteristics of baroclinic Rossby waves. We will demonstrate that the global sea surface temperature (SST) record produced by the Along Track Scanning Radiometer (ATSR) flown on the ERS-1 satellite between 1991 and 1996 contains much evidence of such features in many parts of the world ocean and at many latitudes. Potentially, this is a source of valuable information about the speeds of Rossby waves and their variation with latitude. The satellite SST record also presents an opportunity to determine how the wave speed may vary with longitude within a particular ocean and whether it can also change over time. To extract such information requires the application of selective analytical tools, and the analysis presented in this paper focuses on the observation of slowly moving waves in extra-equatorial regions rather than the faster waves found at and near the equator.

Planetary waves are propagating perturbations in the layered structure of the ocean as the structure adjusts to the disturbance of isopycnal surfaces. Rossby wave dynamics are governed by a restoring mechanism based on the meridional gradient of planetary vorticity. A fluid parcel displaced north or south must adjust its relative vorticity or layer thickness in order to conserve potential vorticity, and in the case of Rossby waves this results in a flow field that tends to restore the fluid to its start latitude. Rossby wave theory [LeBlond and Mysak, 1978; Gill, 1982] demonstrates that this can only occur for waves that travel westward relative to the mean ocean current. Their speed, typically a few cm s^{-1} , depends on β , the latitudinal variation of the Coriolis parameter. Rossby waves are important because they provide a mechanism for transferring information about disturbances across the oceans, typically over a long timescale of order several years. Consequently, a disturbance of the main pycnocline on the eastern side of an ocean, caused, for example, by anomalous winds, may result in the evolution of an eddy or other dynamical feature on the western side of the ocean some years later.

Rossby waves could complete an air-sea interaction feedback loop that gives their propagation characteristics a wider interest to ocean and atmosphere dynamicists and climate scientists. Such feedback could influence the timing and periodicity of quasi-oscillatory features such as the El Niño-Southern Oscillation (ENSO) phenomenon, as suggested by Graham and White [1988, 1990]. Although Kessler [1991]

¹Now at School of Earth and Ocean Sciences, University of Victoria, PO Box 3055, Victoria, BC, V8W 3P6, Canada.

Copyright 2000 by the American Geophysical Union.

Paper number 2000JC900067.
0148-0227/00/2000JC900067\$09.00

could find no linear mechanism for off-equatorial Rossby waves to influence the equatorial waveguide, *White et al.* [1990b] and *White and Tai* [1992] observed reflections of Rossby waves at the margins of the Pacific Ocean, which would be consistent with feedback. In further studies with a coupled model, *Kirtman* [1997] demonstrated that off-equatorial Rossby waves (beyond $\pm 7^\circ$ of the equator) are required to provide a means for the meridional structure of the wind stress anomaly to influence the simulated ENSO period.

Rossby waves may also contribute to the influence of El Niño on global weather and climate. *Jacobs et al.* [1994] found evidence in model-derived and altimeter-derived sea surface height (SSH) of wavelike propagating signals, which corresponded to the expected Rossby wave response to an El Niño event. These appeared to influence the rerouting of the Kuroshio extension after ~ 10 years from the 1982-1983 El Niño, thus impacting SST anomalies over a wide region of the western Pacific. They concluded that the ocean, as well as the atmosphere, has a role in widely broadcasting the climatic influence of what is at first a regionally localized phenomenon. Because the oceanic teleconnection is much slower than the atmospheric teleconnection, it extends the timescale of the response to the decadal.

Recent work by *White et al.* [1998] has further demonstrated, from the analysis of model results and observations, the possibility of coupling between oceanic Rossby waves and the overlying atmosphere. They show that in the eastern central Pacific the anomalous heat flux from ocean to atmosphere balances the enhancement of meridional advection of heat into the region, associated with biennial Rossby waves. *White et al.* also point out that Rossby waves thus coupled to the atmosphere by the thermal feedback between the ocean and atmosphere can be reinforced and that their resulting phase speed may be influenced by the local spatial gradients of the SST field. The phase speed modification includes a meridional component.

Studies such as those outlined above point out the importance of gaining a better knowledge of Rossby wave propagation characteristics in the ocean. Whereas most of the modeling studies of large-scale oscillations between ocean and atmosphere rely on theoretical models of Rossby wave propagation, comparison between theory and observations still shows discrepancies, as reviewed in section 2. In circumstances where the propagation time of an anomaly across the ocean is crucial for determining whether or not an oscillation grows, a knowledge of the actual rather than the theoretical speed is necessary. Thus for the modeling and forecasting of climate variations such as ENSO, having a more complete definition of how Rossby wave speeds vary across the ocean, in both space and time, would be valuable. While the SSH record from satellite altimeters is beginning to provide this, there is a benefit in having an independent alternative approach for detecting Rossby waves, which can be found in the SST record and which may even yield additional information. This forms the subject of this paper. We have discovered that the averaged sea surface temperature (ASST) product of the ATSR provides a readily detectable signature of Rossby wave-like propagation, from which determining the phase speed and its spatial variability, across all the world oceans between the tropics and midlatitudes, is possible. Whilst conceding that the thermal signature of Rossby waves is not such a direct representation of their dynamical characteristics as is the SSH signal, the thermal signature is influential for the processes of ocean-atmosphere interaction.

In the rest of this paper, we first review the measurements of Rossby wave speeds from altimetry and their comparison with theory and discuss previous observations of thermal signatures of Rossby waves. In section 3 we provide details of the ASST data on which the analysis is based and how they have been processed into longitude-time plots, which in section 4 we use to present the evidence for Rossby wave thermal signatures. In section 5 we describe the analytical methods developed to obtain an objective measure of Rossby wave zonal phase speeds from the data, and in section 6 we present the results of these methods. In section 7 we consider separately the latitude dependence of speed as compared with theoretical models and altimeter results, the observed variability with longitude, and the variations with time. The conclusions identify the importance of what has been discovered, pointing out the potential to apply the results more widely and to develop further the analysis of the data.

2. Observations of Extratropical Planetary Wave Speeds

Following the first identification of the Rossby wave mechanism [*Rossby*, 1939], the basic theory of Rossby wave propagation has become well established [*Dickinson*, 1978; *LeBlond and Mysak*, 1978; *Gill*, 1982]. Here we are concerned with long baroclinic extratropical Rossby waves, for which $\kappa_H a_i \ll 1$, where κ_H is the horizontal wavenumber of the planetary wave and a_i is the baroclinic Rossby radius. The magnitude and geographical variation of the first baroclinic mode Rossby radius in various regions has been estimated by *Emery et al.* [1984], *Houry et al.* [1987], and *Picaut and Sombardier* [1993]. Most recently, *Chelton et al.* [1998] have presented ocean-wide maps of its distribution at a resolution of $1^\circ \times 1^\circ$, varying from <10 km at high latitudes to ~ 100 km at 10° and over 230 km at the equator. Thus the thermal anomalies discussed later in this paper must have length scales much larger than this if they are to be considered as long waves. The waves are nondispersive and travel westward at a speed fixed by the environment and independent of the wavenumber or orientation of the waves. The combination of β varying with latitude and a_i varying with both latitude and longitude imparts a strong meridional and weaker zonal variability to the phase speed of the Rossby waves.

While the basic theory has been well established for many years, it has required testing by observations to establish whether (1) the approximations made in the theory are justified or result in significant discrepancies from reality and (2) the Rossby waves propagate freely or are coupled to the atmospheric forcing. Apart from a few localized observations, the original theoretical development was far in advance of the ability to test it on a global scale. Much of the observational evidence for Rossby wave propagation came from the eastern Pacific, where regular transects between Hawaii and California provided the necessary hydrographic data [e.g., *Emery and Magaard*, 1976; *White*, 1977; *Meyers*, 1979; *Kang and Magaard*, 1980; *White and Saur*, 1981, 1983; *Kessler*, 1990]. In the past decade the availability of SSH measurements from satellite altimeters made a useful new contribution. *White et al.* [1990a] found annual Rossby wave characteristics in a year of Geosat data in the region of the California Current. *White et al.* [1990b] and *White and Tai* [1992] went on to study the interaction of annual and interannual Rossby waves at the western boundary, noting their importance in mass redistribution in the tropical Pacific through the reflection of

Kelvin waves. *Jacobs et al.* [1993] were able to find a signal in the Geosat data that matched the wavenumber-frequency relationship of Rossby waves and was significantly above the noise level. By this means they extended the spatial coverage of their analysis to the whole of the Pacific Ocean. *Van Woert and Price* [1993] presented Geosat data as longitude-time plots to reveal the westward propagating signal of planetary waves off Hawaii, while *Tokmakian and Challenor* [1993] and *Le Traon and De Mey* [1994] also displayed SSH evidence of Rossby waves. However, the tidal aliasing in the Geosat altimeter record did not permit a very stringent test of the theory.

Only when satellite altimetry achieved precision at the 2-3 cm level with the advent of the TOPEX/Poseidon mission did it become possible to observe Rossby waves globally, to study their modal structure and behavior in more detail [*Polito and Cornillon*, 1997], and to measure precisely their propagation speed [*Chelton and Schlax*, 1996; *Cipollini et al.*, 1996, 1997]. At last the measurement precision was capable of revealing geographical distributions of wave speed that had not been predicted. Rossby wave speeds, measured with confidence in the TOPEX/Poseidon record, were found to be consistently greater than the theory predicted, even by a factor of ~ 2 at midlatitudes. Such a result provoked a review of the assumptions and simplifications implicit in the earlier theory. *Killworth et al.* [1997] considered a number of factors ignored in the original theory but already shown to influence Rossby waves. These included the response to real bottom topography [*Barnier*, 1988; *Wang and Koblinsky*, 1994], the large amplitude of the waves resulting in nonlinear responses [*Herrmann and Krauß*, 1989], and the presence of steady currents in the ocean [*Gerdas and Wübbler*, 1991], which impart additional vorticity to the flow, thus changing the dispersion relation (effectively the same as locally increasing or decreasing β). They demonstrated that when the theoretical model took into account the presence of an east-west baroclinic mean flow, causing changes in the potential vorticity gradient, the predicted Rossby wave speeds increased, although they remained somewhat less than those observed. The residual discrepancy may be further reduced by taking into account the bottom topography as considered by *Killworth and Blundell* [1999]. Another reason for discrepancy between observation and theory could be that the knowledge of the geographical distribution of the Rossby radius is poor, a subject addressed by *Chelton et al.* [1998].

Given the remaining discrepancy with theory and the wide spread of speeds observed in the altimetry data, using alternative methods for measuring Rossby wave speeds in order to confirm and perhaps to complement the TOPEX/Poseidon data would be valuable. In this paper we describe how satellite measurements of SST can provide a very effective additional means of measuring the speed of planetary waves. This begs the question of whether SST structure is an effective indicator of Rossby wave activity. It could be argued that at best it is a secondary outcome of Rossby waves and not a reliable indicator of whether Rossby waves are truly present or not. There are at least two ways in which baroclinic Rossby waves might acquire a signature in the SST field. First, the compression and stretching of the surface layer when Rossby waves are passing could affect the temperature of the layer. Second, Rossby waves produce a north-south displacement of fluid, which results in temperature changes if there is a meridional gradient of temperature to be advected past the observer. Some of the early experimental evidence of Rossby

waves came from temperature measurements [*Kessler*, 1990; *White*, 1985] and careful analysis of SSTs based on composites of in situ and satellite data [*Halliwel et al.*, 1991a, b]. While the evidence of Rossby waves in SST was searched for in vain by *Van Woert and Price* [1993], *Cipollini et al.* [1997] found a clear thermal signature of Rossby waves at 34°N in the northeast Atlantic. Of particular interest is their discovery that the thermal Rossby wave signature appeared to favor a different mode than the SSH signature. In longitude-time plots from both sources, at 34°N, three distinct baroclinic modes were found. The rank order of the amplitudes of the signals from each mode was reversed between the SSH and the SST signals.

The principle of using SST as an indicator of Rossby waves is therefore well established, although to our knowledge, no previous systematic analysis of a global SST data set has been attempted in order to measure Rossby wave speeds. While we should be cautious of assuming that the SST record can tell us about all the Rossby wave activity, the same can also be said for the use of SSH. Since the baroclinic waves have their greatest action at the thermocline, their sea surface signatures are bound to be dependent on the modal structure. In the case of the thermal signature, modes for which the north-south surface currents are a maximum are likely to be favored as these advect the meridional surface temperature gradients. While this may be a weakness in relation to providing a complete view of Rossby wave activity, it is a clear advantage for those applications where the thermal signature of the waves is important, such as in air-sea interaction processes. As pointed out already, the recent work of *White et al.* [1998] developed a theory of coupled Rossby waves dependent on the meridional temperature gradient. This suggests that we may not always see free waves in the thermal record because the speed of the coupled waves dominates the thermal signature of the Rossby waves. However, the ability to measure these readily would be an advantage since this very speed is what matters for the decadal air-sea interactive feedback processes of importance for climate.

3. SST Data Sources

The global SST data set used for this study is the ASST product derived from the ATSR flown on the ERS-1 satellite. SSTs during the almost 5 year period from August 1991 to April 1996 were obtained from *Murray* [1995] for the first 4 years and from Rutherford Appleton Laboratory's ATSR website for the final 9 months. The ATSR measures SST across a 500 km swath using a conical scanning action that delivers two views of the sea, one viewing forward at an incidence of $\sim 60^\circ$ and the other viewing at near nadir [*Edwards et al.*, 1990]. From the dual views at two or three spectral wave bands, atmospheric correction is applied, and SST is estimated on a grid of 1 km resolution [*Zavody et al.*, 1994]. The ASST product generates estimates of the average SST from the cloud-free pixels within half-degree latitude-longitude cells for each overpass. The orbit pattern ensures at least 1 day and 1 night overpass every 4 days and more frequent overpasses at most latitudes. Monthly averages were produced for each half degree cell and combined into global image data sets of 720×360 pixels, ensuring that there is little drop-out caused by cloud cover. Monthly time resolution should be adequate to define a signal traveling as slowly as an off-equatorial Rossby wave, given the relatively coarse spatial resolution. The accuracy of SST recovered from the ATSR has now been

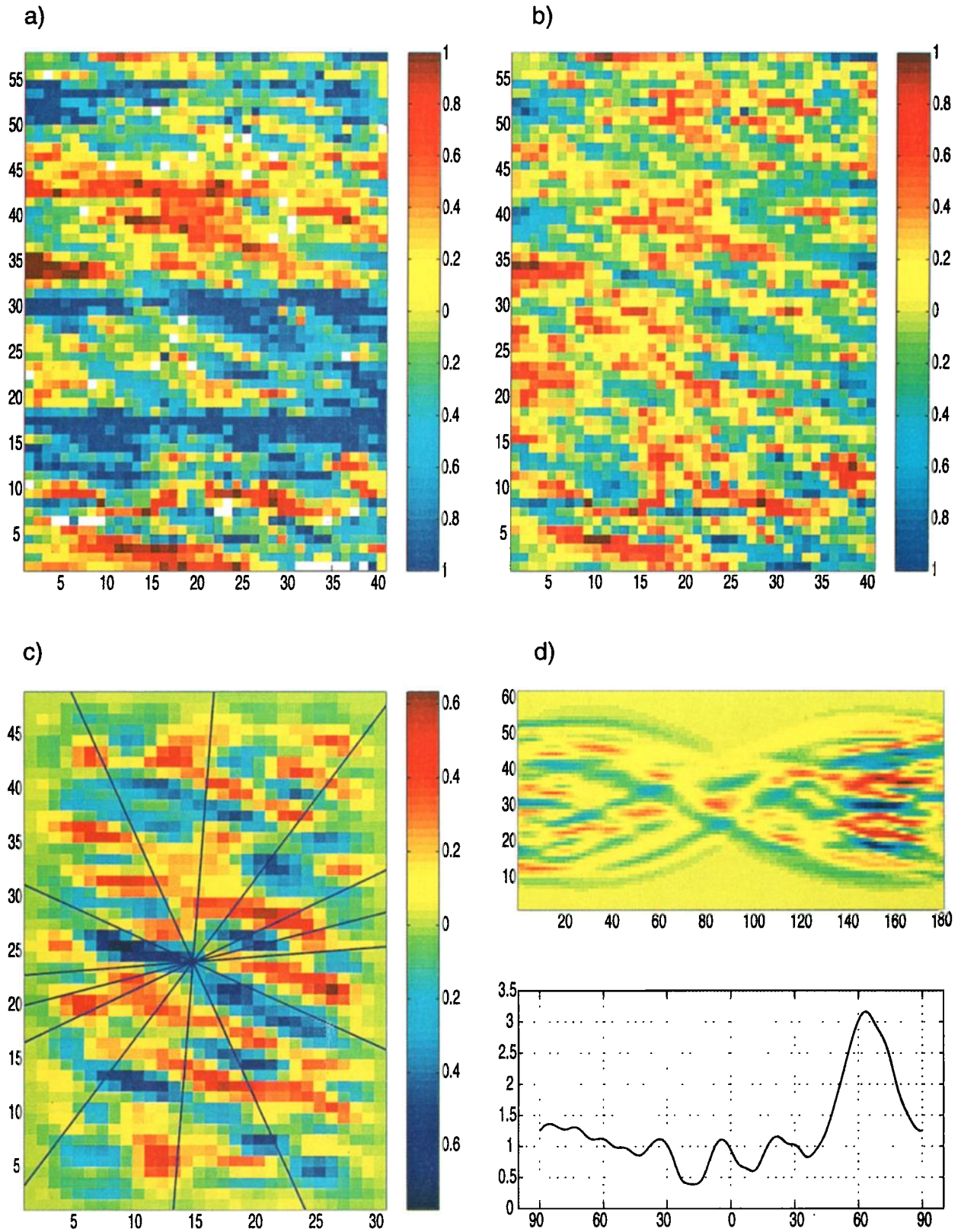


Plate 1. Stages in the application of the Radon transform applied to an example centered at 95°E , 25°S : (a) the original 40×48 window, (b) the window after removal of outliers and monthly striping, (c) window after application of band-pass and tapered filter, and (d) plot of the standard deviation of each column in the Radon transform against orientation of the baseline. The peaks correspond to the lines drawn in Plate 1c with the maximum peak in bold.

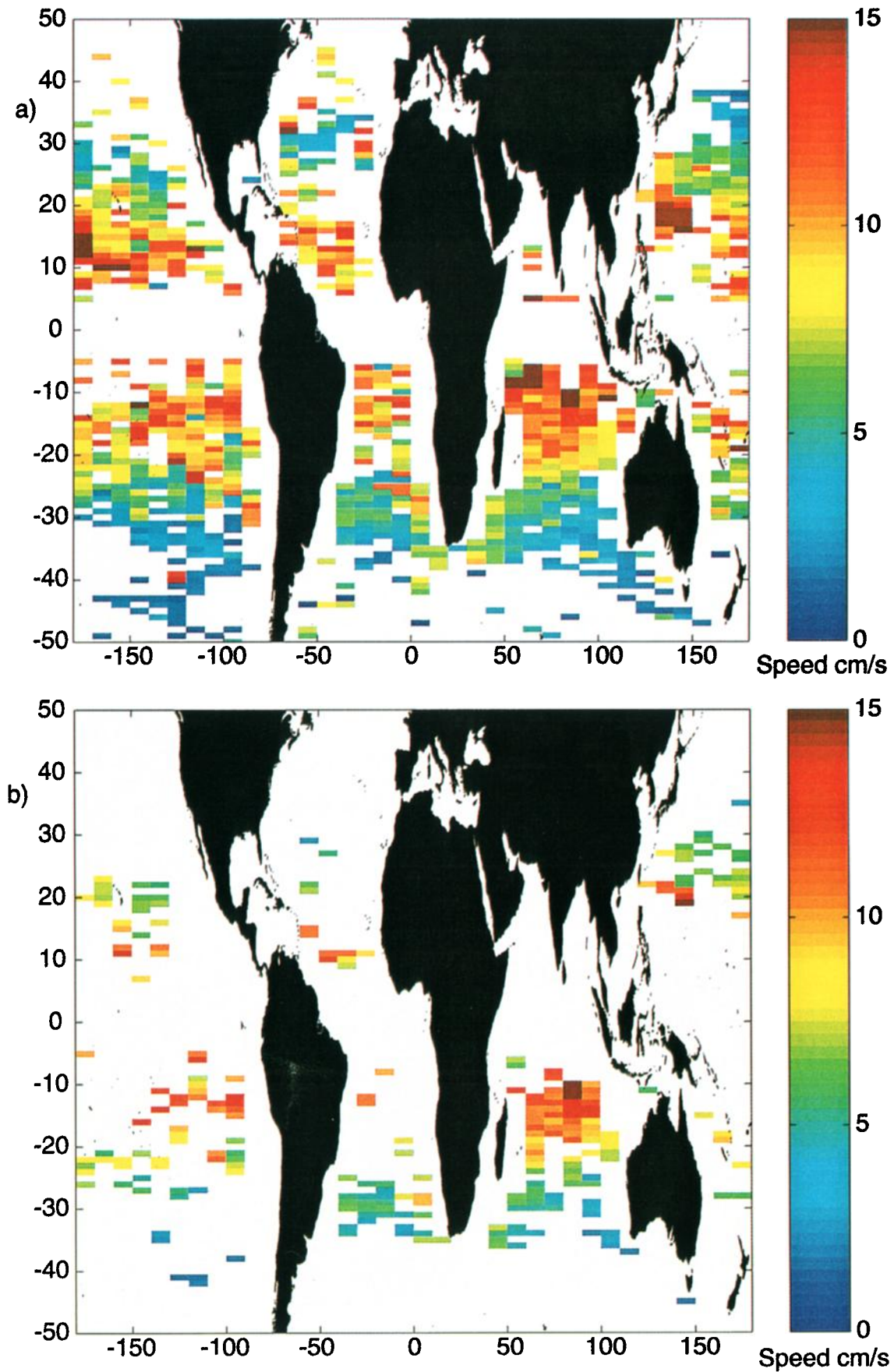


Plate 2. (a) Map of phase speeds (strongest peak for westward propagation) with a peak-to-average standard deviation ratio threshold of 1.8 and (b) map of phase speeds with a ratio threshold of 2.3.

validated by a number of authors [Mutlow *et al.*, 1994; Závody *et al.*, 1995; Barton *et al.*, 1995]. ATSR appears, in general, to be achieving its intended accuracy of 0.3 K except during periods of exceptional volcanic activity when stratospheric dust introduces a cool bias that is expected to be removable following further tuning of the algorithms [Murray *et al.*, 1998].

In principle, the ASST data should be considerably more accurate than 0.3 K since each averaged value can come from ~2500 individual 1 km² pixels. Donlon and Robinson [1998] compared the ASST with coincident ship radiometer measurements of skin temperature in the North and South Atlantic. They found a variance of only 0.2 K in the match, although there was a bias of 0.5 K ascribed to stratospheric volcanic dust corrupting the atmospheric correction procedure at the time of comparison. The low variance implies low noise in the ASST data product. Although Jones *et al.* [1996a, b] found that the ASST data set was corrupted by undetected daytime cloud in parts of the ocean, leading to a cool bias in a few locations, this should not be a serious problem here since we will search for temperature structures in the data. These propagate at a given speed and are unlikely to be aliased by the effect of poor cloud screening. We therefore selected the monthly composites of ASST derived from all (day and night) overpasses.

In order to isolate possible SST signatures of planetary waves from the regular variability of the seasonal cycle the SST anomaly distributions for each month were evaluated by subtracting a climatic mean SST field for each month of the year. At first the mean derived from the ASST data set itself was tried, but not only was this too short a record, but it also contained a regular pattern of drop-outs at low latitudes from the periods when ERS-1 was following a strict 3 day repeat orbit. Instead, the global ocean surface temperature atlas (GOSTA) climatic monthly mean SST data were used [Bottomley *et al.*, 1990]. This is derived as a bulk SST from 30 years of ship and buoy data collected between 1951 and 1981, and it contrasts with the skin SST measured by ATSR. However, any bias introduced by this or by other causes, such

as sampling differences within the half-degree grid cells, is not a problem since the spatiotemporal variability of the SST anomaly rather than its absolute value is what is of interest here. Figure 1 shows an example of the ASST-GOSTA anomaly field for April 1992. Wave-like perturbations of SST are apparent in several parts of this image, but a single image cannot reveal whether or not these are propagating features. To do that the time series must be examined, as explained in section 4.

4. Longitude-Time Variation of SST

The variation with time of the ASST record at a given latitude is revealed in longitude-time plots such as Figure 2, sometimes called Hovmüller diagrams. Centred at 32°S, each row of this plot has been produced by averaging the SST from two adjacent half degree latitude slices (31.5°-32°S and 32°-32.5°S) from an anomaly image, preserving half degree resolution in longitude. Each zonal slice is obtained from one of the sequence of 45 monthly anomalies and stacked up vertically with time increasing upward. The vertical blocks of null data correspond with where the selected latitude slice intersects the continents. A geometrically regular pattern of thin lines of null pixels in months 1-8 and 30-32 corresponds to the gaps in coverage during the 3 day repeat cycle of ERS-1.

Figure 2 clearly shows a pattern of diagonal stripes which trend from bottom right to top left. Their width is a few degrees of longitude, and their thermal amplitude varies between ~0.1 and 1.5 K. They are readily distinguished from other features, such as the null pixels, the horizontal lines of high or low anomaly resulting from an anomalously warm or cold month, and other random fluctuations of temperature whether localized or extending over a wide region of longitude-time space. The fine stripes indicate east to west propagation of SST anomaly perturbations along 32°S. Their coherence approaches that found in the SSH record. They are pervasive both spatially and over time, implying that SST perturbations can be found on many occasions throughout the 45 month data record, and may propagate right across entire

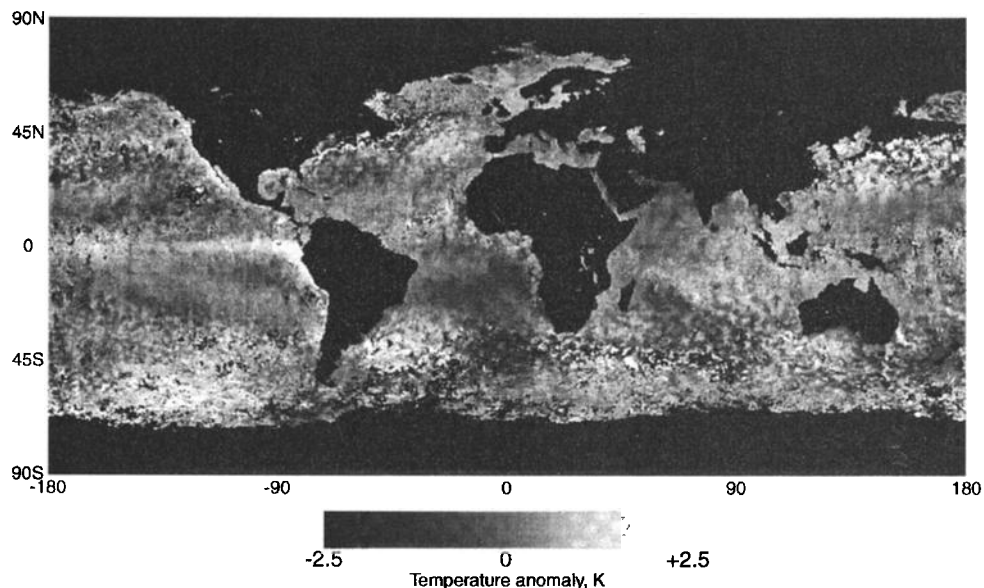


Figure 1. Sea surface temperature monthly mean anomaly from April 1992 ASST-GOSTA.

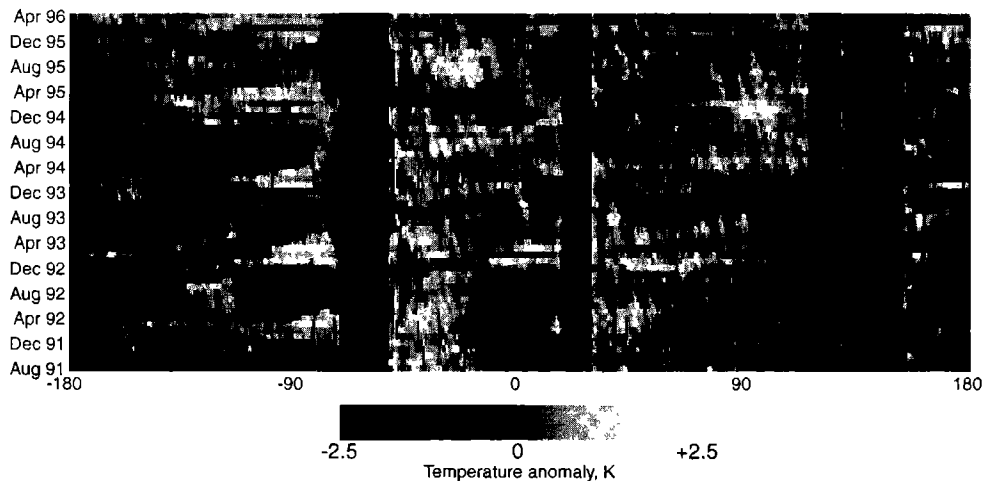


Figure 2. Longitude-time plot of ASST-GOSTA anomaly at 32°S. In this as well as in the following longitude-time plots the temperature digitization interval is 0.02 K.

ocean basins. The approximately parallel nature of the patterns indicates a steady propagation speed, which is similar at most longitudes and in each ocean, although by no means uniform, as will be discussed later. The regularity of the patterns implies that these are dynamically controlled features rather than random perturbations. The most satisfactory explanation is that they represent the SST anomaly signatures associated with dynamical disturbances that propagate westward as Rossby waves.

Examination of the Hovmöller plots from other latitudes (see Figure 3) confirms that 32°S is not exceptional in revealing such signatures. At 30°N (Figure 3a) the anomaly signal is somewhat noisier close to both the east and west margins of the Pacific, and more null pixels result from cloud cover, but the westward propagating regular perturbations remain a dominant feature of the variability. At 22°N (Figure 3b) the signatures continue to dominate the Pacific Ocean, although they are weak or disappear altogether in the Atlantic. At 36°S (Figure 3c) the wave-like signature is strong in all oceans, but at this latitude the slope of the features appears to vary considerably, both with longitude and with time. At lower latitudes, especially <math><10^\circ</math>, the phenomenon becomes much harder to detect. Figure 3d is an example from 8°S showing an almost featureless Pacific, although some wave-like features are still found in the Atlantic and Indian Oceans. These have shallow slopes, i.e., faster speeds.

The examples already presented are representative of all the other Hovmöller plots of SST anomaly that have been examined at 1° intervals of latitude between 5° and 50° north and south. The overall conclusion from a qualitative analysis is that the ASST-GOSTA anomaly maps contain a considerable quantity of information about the propagation of SST perturbations at length scales of 200–2000 km. The speed of propagation appears to be regular and to vary systematically with latitude, increasing as the equator is approached. The speed varies to a lesser extent with longitude. The speed of propagation was initially estimated approximately by directly measuring the slope on the Hovmöller diagrams at different latitudes and in the different ocean basins. These estimates are plotted in Figure 4 along with the meridional variation of the zonal average speeds of the first baroclinic mode Rossby wave predicted by the modified theory of Killworth *et al.* [1997].

The general similarity is striking, although there are clearly some discrepancies between the speed of the SST features and the Rossby wave theory. From this evidence alone, supposing that these features are the thermal signatures of planetary waves is reasonable. This hypothesis is developed further in the remainder of this paper.

Of course, the idea that Rossby or planetary waves should be detectable by their thermal signature is by no means new, as some of the literature discussed above makes clear. Nonetheless, what is surprising is the clarity of the features in the ASST record and their ubiquity throughout much of the ocean and at many times of the year. The apparent coherence of the troughs and crests of the features over many months and across thousands of kilometers is consistent with the signature of Rossby waves in the altimeter record [see, e.g., Chelton and Schlax, 1996; Cipollini *et al.*, 1996]. Moreover, the global satellite SST record appears to be a source of valuable information about the low-frequency dynamics of the ocean that has hitherto been overlooked.

Does only the ASST data contain such information? Figure 5, a longitude-time plot constructed for 32°S from the Advanced Very High Resolution Radiometer (AVHRR)-derived SST anomalies by A. Strong (Oceanic Research and Applications Div. of NOAA), reveals that this is not the case. The wave-like features are clearly evident here too, although an examination of the complete AVHRR data set at all latitudes found that the features are more readily identified within the ASST than within the AVHRR because of the former's finer precision and lower instrument noise. We note also that there is no need to look to the zonal gradient of temperature for the signatures of planetary waves, as previous authors [Hughes, 1995, 1996; Cipollini *et al.*, 1997; Hughes *et al.*, 1998] have tended to do in order to remove the local residual annual signal.

Before turning to a more systematic and objective analysis of the phenomenon, one other feature in the Hovmöller plots is worth pointing out. This is illustrated in Figures 6a and 6b, the ASST-GOSTA Hovmöller plots for 40° and 48°S, respectively. Here we see strong evidence for features traveling in the eastward direction, in the Indian sector of the Southern Ocean. Regions to which waves converge, from which they diverge, and even where the features appear to be

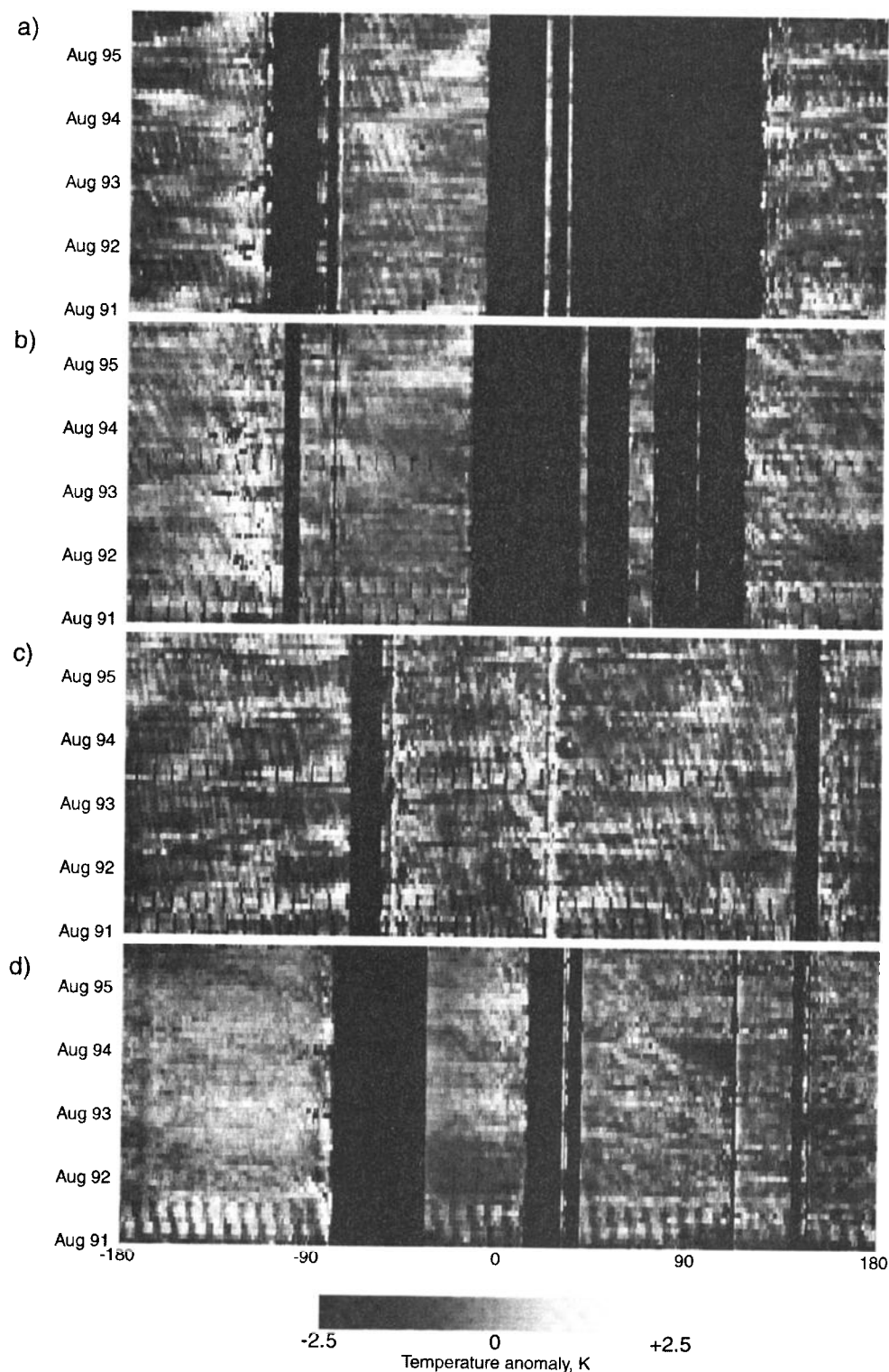


Figure 3. a) Longitude-time plot of ASST-GOSTA anomaly at 30°N, (b) longitude-time plot of ASST-GOSTA anomaly at 22°N, (c) longitude-time plot of ASST-GOSTA anomaly at 36°S, and (d) longitude-time plot of ASST-GOSTA anomaly at 8°S.

static are evident. At other longitudes the features are consistent with all the other plots. Supposing that this may be related to the eastward advection at the depth of the thermocline by the Antarctic Circumpolar current at 48°S [Hughes, 1995, 1996] and to the propagation of eddy-like features in the Agulhas retroflection at 40°S is reasonable, although more detailed inspection is called for.

5. Analytical Methods

The significance for dynamical oceanography of the features discussed above is their potential to provide a method for directly measuring the speed of planetary waves. Although the results of preliminary analysis simply using eye and ruler were promising (as in Figure 4), such an approach is too

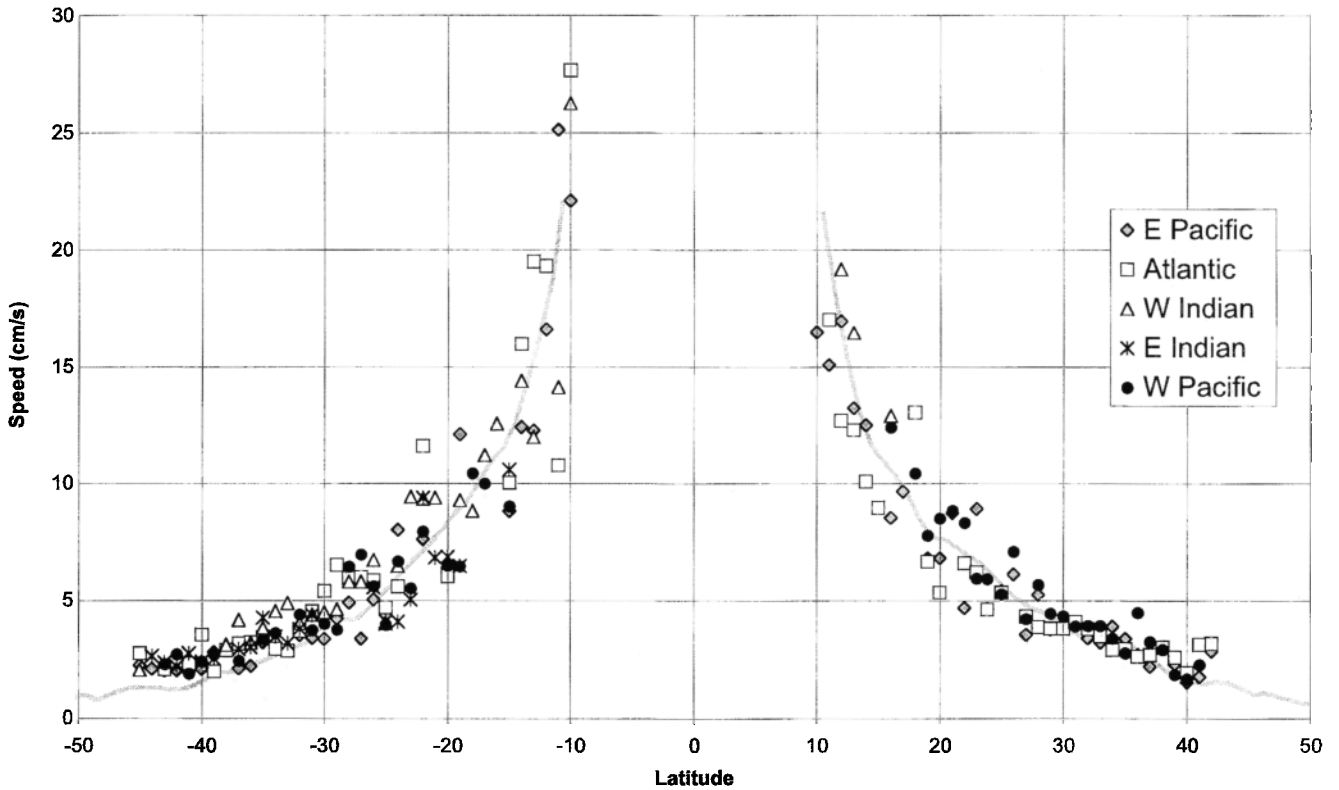


Figure 4. Preliminary estimates (by eye from ASST-GOSTA longitude-time plots) of Rossby wave speed plotted against latitude.

subjective to be capable of yielding repeatable results from independent analysts. An objective analytical tool is therefore needed to derive the speed of the waves. Previous analysis of both the thermal and altimetric signals has approached the problem by first measuring the spatial and temporal frequencies of the Hovmüller patterns using Fourier analysis and thence the phase speed from the ratio of frequency to wavenumber. The difficulty of such an approach is that although the human eye picks out the linear stripes readily, the application of Fourier transforms to the noisy data only yields encouraging results where the waves are sufficiently coherent in wavenumber and frequency and show a clear

periodicity. Moreover, even where the patterns are strongest and most regular, other features of comparable magnitude might be adding energy to the image variability at frequencies similar to those of the waves being studied. Errors in both wavenumber and frequency can lead to large errors in phase speed estimates.

Conversely, even where the frequency and wavenumber of the features is ambiguous or variable, the strong characteristic of the patterns is their linear coherence and locally parallel nature. Therefore using a numerical analysis tool that can measure the slope or direction of the linear features directly makes sense. Accordingly, we have developed a method that

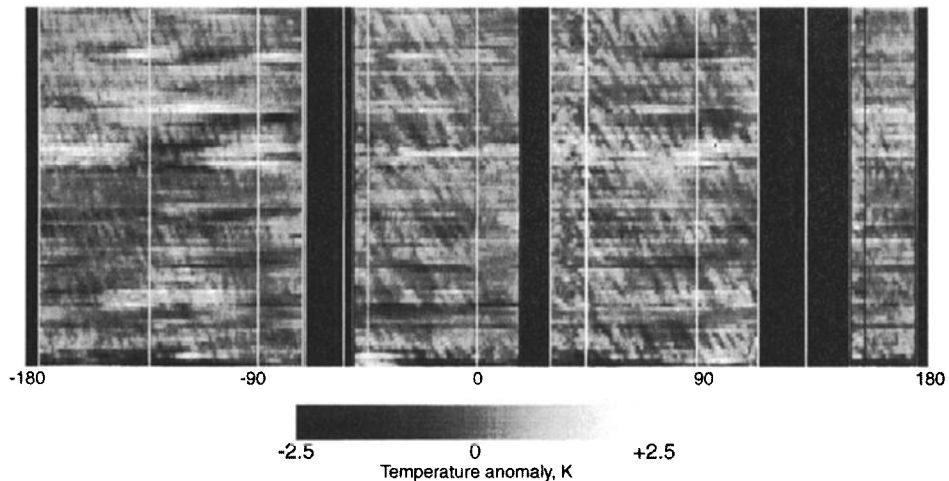


Figure 5. Longitude-time plot of AVHRR SST anomaly at 32°S.

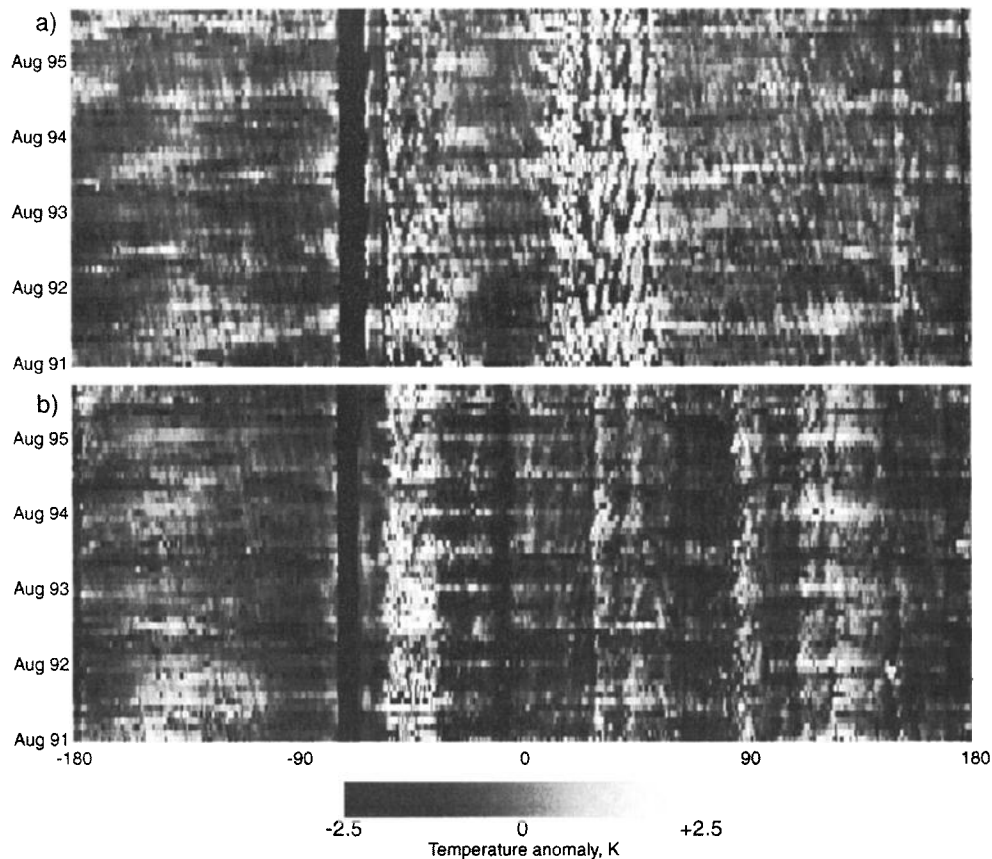


Figure 6. a) Longitude-time plot of SST anomaly at 40°S, and (b) longitude-time plot of SST anomaly at 48°S.

is based on the concept of the two-dimensional Radon transform [Radon, 1917; Deans, 1982]. Chelton and Schlax [1996], Cipollini *et al.* [1996], and Polito and Cornillon [1997] have already demonstrated the use of a Radon transform to measure phase speeds of Rossby waves. The Radon transform operates on a window within the longitude-time image by summing the pixels along perpendiculars to a baseline of a given orientation θ (see Figure 7). If the baseline is orthogonal to the striping in the image, the resulting Radon vector will be highly variable. In contrast, if the baseline is parallel to the striping, the perpendiculars will cut across the variability in the image, and the resulting Radon vector will have low variance. The full Radon transform is created from the matrix of all orientations θ of the baseline. The task for automatic direction-detecting software is to find the orientation of baseline that yields the maximum variance in the Radon transform. The following is the procedure which was adopted.

1. A window is isolated from the longitude-time plot. The size of this is adjustable, but for the results presented here, 20° longitude (40 columns) by the entire time span of the data, i.e., 57 months (rows), is used. To illustrate the process, Plate 1a shows an example of the data centered in the Indian Ocean at 95°E, 25°S viewed through a 20° (40 column) by 48 month window.

2. The outliers in each row are removed. These are identified as values that are outside the row mean ± 2 standard deviations of the row.

3. To remove the effect of individually strong monthly anomalies that would otherwise dominate the striping in the

window (as visible in Plate 1a), the mean of each row is subtracted from the row (recomputed after step 2). This also has the effect of ensuring that the mean of the whole window is zero.

4. Any missing values in the window (resulting from cloud, ERS-1 orbit pattern, or step 2) are replaced using a Gaussian interpolator having a full width at half maximum of 1° longitude and 0.2 month time and a search radius of 1.5° longitude and 1 month in time. The result is shown in Plate 1b.

5. The window is then convolved with a two-dimensional band-pass filter designed to remove the high-frequency noise and the residual large-scale variability. The (idealized) passband of the filter is the region in frequency space between two ellipses centered in the origin, whose intersections with the wavenumber axis are $1/7.5^\circ$ and $1/2.5^\circ$ and with the frequency axis are $1/18$ per month and $1/3$ per month. The real filter to achieve this has a 21×21 kernel and somewhat smoothed sides.

6. After the band-pass filtering the window is cropped to $15^\circ \times 48$ months. Reducing the width improves the longitudinal resolution. The first 8 months were discarded because they contain sampling artefacts resulting from two periods of exact 3 day repeat orbit cycles, leaving gaps in coverage at low latitudes. The last month is also discarded.

7. The resulting 30 column \times 48 row matrix is tapered using a window of the same size having a unit value at its center and the five elements along each border varying from 0 at the outside to 1 as raised cosines (like the sides of a Hanning window). This minimizes the effects of the rectangular shape

of the matrix to be analyzed, which would otherwise generate unwanted undulations (lobes) in the Radon transform and spurious peaks in its standard deviation. The band-pass filtered and tapered matrix is shown in Plate 1c.

8. The Radon transform is performed for θ varying from -90° to 90° in steps of 1° , and its standard deviation is computed for each θ . Both the transform and its standard deviation are shown in Plate 1d.

9. The values of θ in the local maxima of the standard deviation correspond to the orientation of the alignments in the longitude-time plot and thus give an objective measure of the speed of propagation of the characteristics. These maxima are identified automatically, converted into propagation speeds, and saved. Also saved is the relative height of the peak defined as the ratio of the standard deviation at the peak to the average standard deviation across all the sampled directions. In Plate 1c, lines are drawn at angles corresponding to each of the maxima in Plate 1d. The strongest peak at $\theta = 63^\circ$ (drawn as a thick line in Plate 1c, and corresponding to a propagation speed of 3.8 cm s^{-1}) is a good match for the most evident propagating features in the longitude-time plot.

The programme moves the window systematically through each Hovmüller plot, producing a new Radon transform every 10° of longitude and every degree of latitude, populating point by point a matrix that determines how the speed of

propagating features varies with longitude and latitude. The filters used in the above method were selected after extensive trials with artificial data, which will be reported in detail elsewhere. These demonstrated the capacity of the method to identify accurately several overlaid linear features in a noisy image, even when they were no longer evident to the eye. The resolution and accuracy with which speed can be estimated depends on the spatial and temporal resolution of the original global SST maps, the size and shape of the sampling window into the Hovmüller plot, the speed itself, and the angular increments over which the Radon transform is evaluated. The tests with artificial data indicated that use of the parameters defined above yielded speed estimates well within $\pm 5\%$ of the given value, except at speeds $>10 \text{ cm s}^{-1}$ when the monthly time sampling is too infrequent to discriminate the speed accurately. The adoption of a 1° incremental interval for evaluation of the Radon transform leads to quantization of the detected speeds at a level that increases nonlinearly with speed and is $\sim 1 \text{ cm s}^{-1}$ at speeds of 10 cm s^{-1} . However, a finer angular resolution of the Radon transform is not justified by the resolution of the original data.

6. Results of Wave Speed Analysis

Plate 2a presents the geographical distribution of the strongest westward propagating signal observed by the Radon

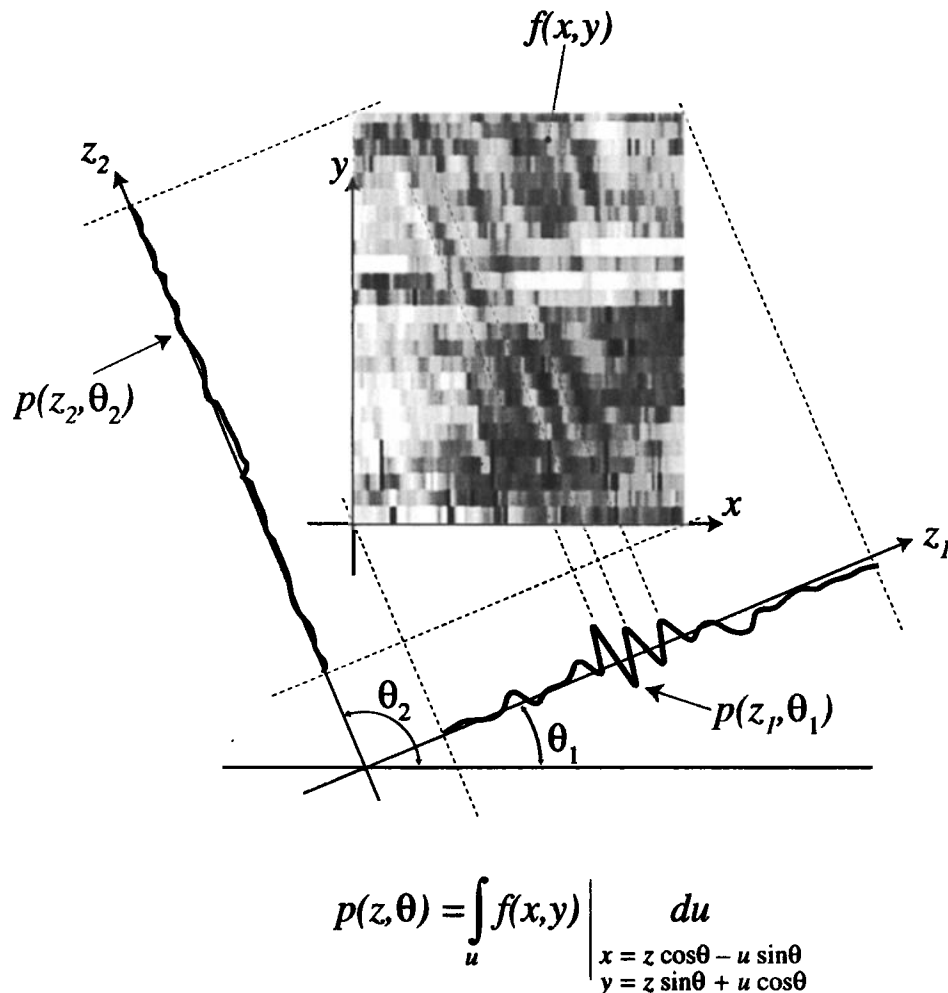


Figure 7. Illustration of the Radon transform of a function $f(x,y)$ at two different angles θ_1, θ_2 .

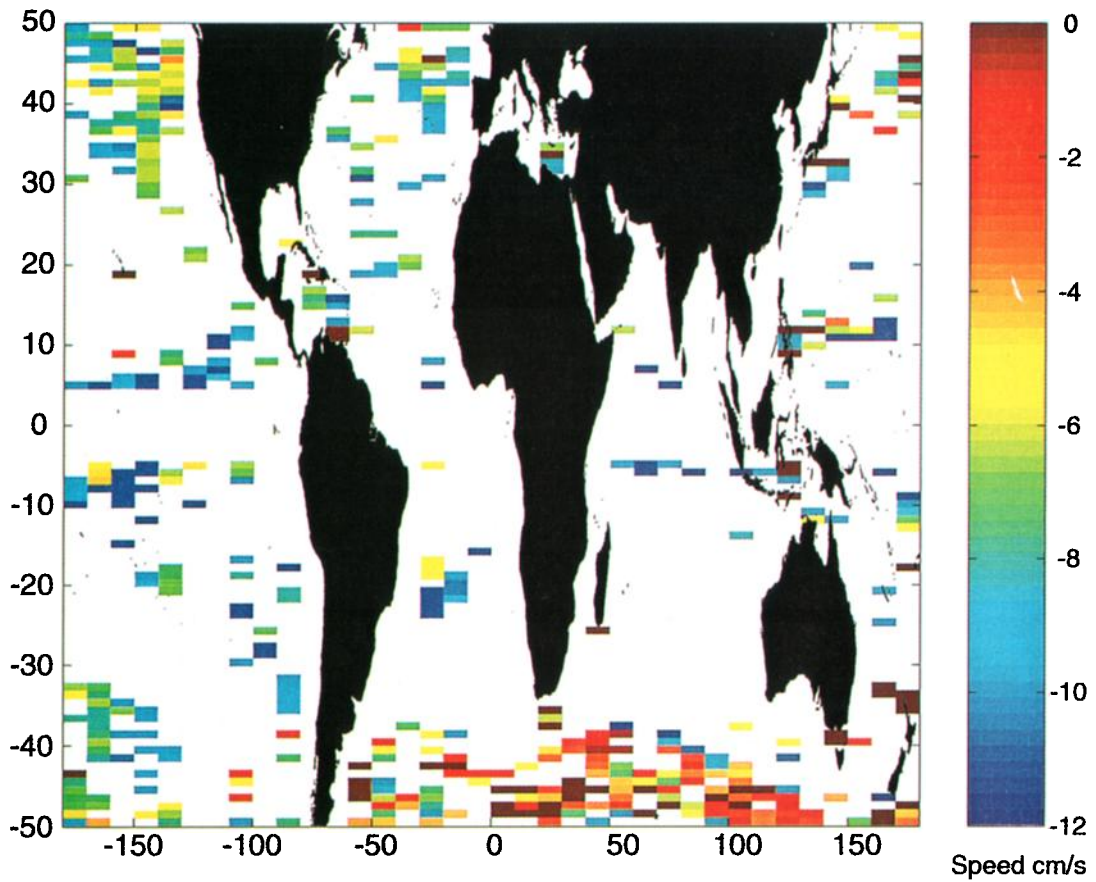


Plate 3. Map of the speed of eastward propagating wave-like features where these were detected.

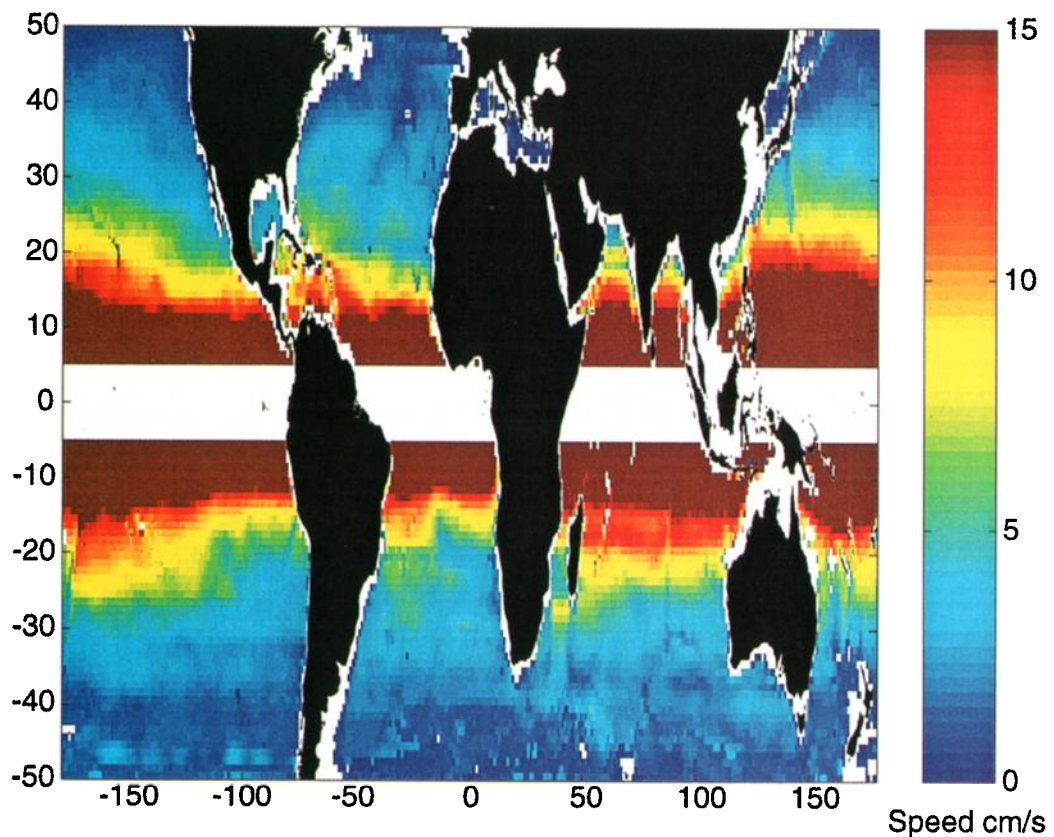


Plate 4. Global distribution of Rossby wave speed predicted by theory of Killworth *et al.* [1997].

transform, evaluated at intervals of 1° of latitude and 10° of longitude. The colors represent the detected speed. A white blank represents a null result because sea data within the 20° longitude window were insufficient or because that area lies outside the examined latitude range of 5° - 50° . Null results were also entered in cases where the signatures were only weakly detected in the Radon transform. As outlined above, the method will always find a peak in the plot of standard deviation against orientation; even where there are no genuine features, the noise in the data will generate peaks, although these are not generally as pronounced as for planetary wave features. The ratio of peak to average standard deviation was used as an objective means to discriminate between the detection of genuine features and spurious artefacts of the method. For Plate 2a a threshold of 1.8 has been adopted. If the peak-to-average standard deviation ratio was less than this, a null entry was recorded.

A number of characteristics can be identified. First, in some regions of the world ocean, for example in the south midlatitude of all the oceans (30° - 38° S), a broad uniformity is found in the measured wave speed that does not vary by more than a few percent between neighboring cells. This implies that the method for determining the wave speed is capable of delivering consistent results in favorable conditions where the wave thermal signatures are clearest. That the speed measurement in each cell is completely independent of its north or south neighbor and overlaps only with its immediate east or west neighbor should be emphasized.

Second, the trend with latitude displayed in the preliminary analysis of Figure 4 is confirmed: increasingly higher speeds are found toward the equator. However, this is not uniformly so since equatorward of $\sim 20^\circ$, a much greater variability in the detected speeds exists. For the most extreme cases the speed measured in adjacent areas may vary between 5 and 12 cm s^{-1} . Third, some evidence of speed variation with longitude exists in particular oceans, with a tendency for speed to increase toward the west, e.g., South Indian and North Pacific Oceans. Finally, the null results, where no strong features are identified, are regionally clustered, particularly in the vicinity of major frontal currents such as the Kuroshio, Gulf Stream, and Antarctic Circumpolar Currents. These are regions where the thermal signature is expected to be dominated by the frontal structure and where planetary waves, even if they exist, are unlikely to have a clear SST signature.

Note that in some locations several strong peaks are found in the Radon transform (e.g., Plate 1d), implying that more than one type of wave may be present, but only the highest peak between $0^\circ < \theta < 90^\circ$, corresponding to the strongest westward signal, has been plotted. A peak found at a negative angle corresponds to an eastward propagating signal. Where the eastward peak is higher than the highest westward peak, indicating a dominant eastward signal, its speed has been plotted in Plate 3 for latitudes south of 30° S. Note particularly the cluster of points in the Southern Ocean appearing south of the Indian and Atlantic Oceans.

7. Discussion

7.1. The Detectability of Westward Propagating Signals

Before seeking to understand the significance of the wave-like phenomena detected in the global composite SST fields

and to establish their relevance to the dynamics of Rossby wave propagation, we should first consider the constraints inherent in the approach. For example, the use of SST obviously limits us to observing only those dynamical processes that have a surface thermal signature. Additionally, the half-degree-monthly space-time sampling frequency of the data set imposes its own limits on the range of speeds that can readily be detected.

Because the data are sampled only once per month, the method is less able to detect faster waves. At 20° latitude a wave traveling at 10 cm s^{-1} will take ~ 4 months to traverse the 10° longitude width of the untapered section of the Radon transform window. Its characteristic signature on the 1 month by 0.5° Hovmüller grid makes an angle of $\sim 11^\circ$ to the horizontal and intersects four rows, making it readily detectable. However, for greater speeds the characteristic approaches the horizontal and is less easily resolved unless either the time-sampling interval is reduced or the longitude window for the Radon transform is increased. The former is not possible with the data set used. The latter was not performed because any improvement in resolution would rely on the uniformity of the signal across 20° or 30° of longitude and would be won at the cost of degrading the longitude resolution. For that reason, no attempt was made to study the equatorial region using this data set. Speeds of 10 cm s^{-1} or above, while detectable, are resolved to no better than 10%. Higher precision of speed measurement within 10° longitude of the equator requires an SST data set with finer temporal resolution.

In locations where more than one mode of Rossby wave occurs and has a surface thermal signature, other modes will give rise to additional peaks. If a slower mode appears more clearly on the Hovmüller plot, it will generate the highest peak on the standard deviation plot. Thus the detected speeds presented in Plate 2 may sometimes be those of modes other than the fastest. This is particularly likely at lower latitudes where the expected fastest modes can barely be resolved.

The choice of 1.8 as a threshold peak-to-average standard deviation ratio for eliminating the lower peaks seems to have excluded most but not all anomalous speed values from Plate 2a. The remaining anomalous values giving rise to apparently random fluctuations of speed in some parts of the ocean might correspond to other dynamical phenomena (like eddies) or chance alignments of SST anomalies not related to deeper propagating features. In an attempt to eliminate such points from the comparison between observed planetary wave speeds and theoretical predictions, a higher threshold of 2.3 was imposed. This has the result of eliminating a number of points that appear to be genuine planetary wave signatures but ensures that the number of spurious points is minimal. Plate 2b shows the corresponding speed distribution with the higher threshold applied.

The mechanisms by which Rossby waves could form a surface signature were mentioned earlier in section 2. The hypothesis of advection of the north-south gradient seems to be the more likely as the Rossby wave signatures are clearest in the region of 25° - 40° S. The signal analysis was able to detect features with fairly consistent speeds across this range, where there is a steep increase of the background SST field toward the equator. Where the meridional temperature gradient is reduced, for example, in western boundary currents, the detectability of the waves was poorer, and the speeds of signals detected by the method were more variable, consistent

with the hypothesis that no strong features exist in the data there.

The limitations identified here must qualify any information about Rossby wave kinematics that is drawn from the observations. Nonetheless, the problem of detecting the faster waves should be considered as a consequence of the monthly sampling of the original data rather than a weakness of the method itself.

7.2. Variation With Latitude

The initial analysis (Figure 4) showed promising, if imperfect, agreement between the variation of our detected wave speed with latitude and the theoretical predictions of *Killworth et al.* [1997] for the first baroclinic mode Rossby wave. A more thorough comparison, allowing for the longitudinal variability of the Rossby wave speed, can be made between Plates 2 and 4, which is the global distribution of Rossby wave speed using the *Killworth et al.* [1997] model. Some correspondence exists between Plates 2 and 4, with higher speeds detected from the SST signature in regions where the model predicts similarly high speeds. The major discrepancy is that in the tropical regions the observed speeds are not uniformly high and the speed does not fall off as rapidly toward high latitudes as predicted by the theory.

This is clarified further in Figure 8a where the wave speeds measured from the SST record are plotted against latitude and compared with the zonal mean wave speed from the *Killworth et al.* [1997] model. Only peaks above the threshold of 2.3 have been plotted. Figure 8a shows clearly the quantization of the speed estimates, particularly at values $>8 \text{ cm s}^{-1}$, resulting from the evaluation of the Radon transform at discrete angles, as mentioned in section 5. The trend with latitude is very clear and in broad agreement with the theoretical predictions. While the spread of points is wide, so to a lesser extent is the longitudinal variability of the theoretical predictions, which are plotted in Figure 8b for the same locations.

Figure 9 makes a direct comparison between the observed wave speeds and the theoretical prediction corresponding to the same location, differentiating between the signatures having a peak ratio between 2.3 and 2.4 and those above 2.4. The overall indication is that the observed speeds are greater than those predicted for speeds $<6 \text{ cm s}^{-1}$, and less than those predicted at higher speeds. At speeds $>6 \text{ cm s}^{-1}$, corresponding approximately to latitudes lower than 25° , the underestimate of observations relative to theory may be a consequence of the analysis method and the coarse temporal resolution of the original data, which make it difficult to measure high speeds accurately. For example, if more than one mode of wave is present in the Hovmüller plots, the method may preferentially detect slower modes rather than the fastest mode if it is of order 10 cm s^{-1} or greater. Moreover, the first mode may have a weaker thermal signature than a higher, slower mode. This would be consistent with the experience of *Cipollini et al.* [1997], who found mode 3 to have the greatest energy in the thermal signature of Rossby waves while mode 1 was strongest in the altimeter record.

However, the mode uncertainty is not able to account for the observed speed being greater than the theoretical zonal mean first mode Rossby wave speed. This is consistently the case at latitudes $>20^\circ$ and speeds $<7 \text{ cm s}^{-1}$. Some care is needed when comparing with the zonal mean, which averages theoretical predictions from all locations irrespective of

whether Rossby waves actually occur there. Reference to Figure 8b indicates that the theoretical speeds for those waves that are isolated by our analysis are also somewhat higher than the zonal mean. Nonetheless, the direct comparison at specific longitudes that is made in Figure 9 still suggests that the theory underestimates the speed by 20-30%.

This reinforces the importance of attempts to revisit the theory, such as *Killworth and Blundell's* [1999] examination of the effects of bottom topography on the speed of extratropical planetary waves. Their calculations confirmed an increase of propagation speed on westward and equatorward sides of hills, but they concluded that local topographic effects largely cancel on basin scales and that the mean flow remains the strongest candidate to account for faster observations. Another possibility is that those waves that have a thermal signature are not propagating freely but, constrained by air-sea interaction feedback processes, acquire different kinematic properties as bound waves, as discussed by *White et al.* [1998]. In that case they would no longer be useful in providing surface signatures of classical Rossby waves but, instead, would be important in monitoring propagating SST features in their own right.

7.3. Variation With Longitude

Figure 8a demonstrates a wide spread of speed with longitude for most latitudes. Reference to Plate 2a reveals a tendency for the observed speeds to increase toward the west of some oceans at certain latitudes, in broad agreement with the theoretical predictions of *Killworth et al.* [1997] in Plate 4. A good example can be found at 32°S on the Hovmüller diagram (Figure 2). While some of the variations may be the result of detecting different modes, as discussed in section 7.2, strong longitude variability is found at the lower speeds that are well resolved by the sampling characteristics of the method and unlikely to be compromised. The ASST record therefore appears to provide a useful means to observe the longitude variability of Rossby wave speed at midlatitudes.

Reexamining longitude variability in the Hovmüller plots in relation to the bottom bathymetry is instructive. Figure 10a, at 27°S , has the matching zonal transect of ocean depth plotted underneath from which connections between speed and major bathymetric features can be detected. Changes of speed (i.e., the slope of the patterns) as well as other propagation anomalies appear at some major ridges. In the Atlantic Ocean we observe a phase discontinuity across the Mid-Atlantic Ridge at 20°W ; the wave propagates smoothly until it reaches the ridge where it appears to be delayed before moving on. In the eastern Pacific, Rossby waves appear to originate over the wide East Pacific Rise area around 120°W , while in the Indian Ocean we see some effects on phase associated with the 90°E ridge and the Central Indian Ridge. In the Indian Ocean, waves appear to be almost completely dissipated at the Madagascar Ridge around 45°E . At 20°S (Figure 10b) a similar pattern of generation just west of the East Pacific Rise and dissipation over the mid-Indian ridges are apparent.

These observations can be related to the quasi-geostrophic modeling studies by *Barnier* [1988] in which the introduction of a ridge into a previously flat ocean showed that the ridge can both block Rossby waves and also support their generation by wind forcing. Similarly, *Herrmann and Krauß* [1989] produced quasi-geostrophic model results suggesting that annual Rossby waves originating at the western boundary

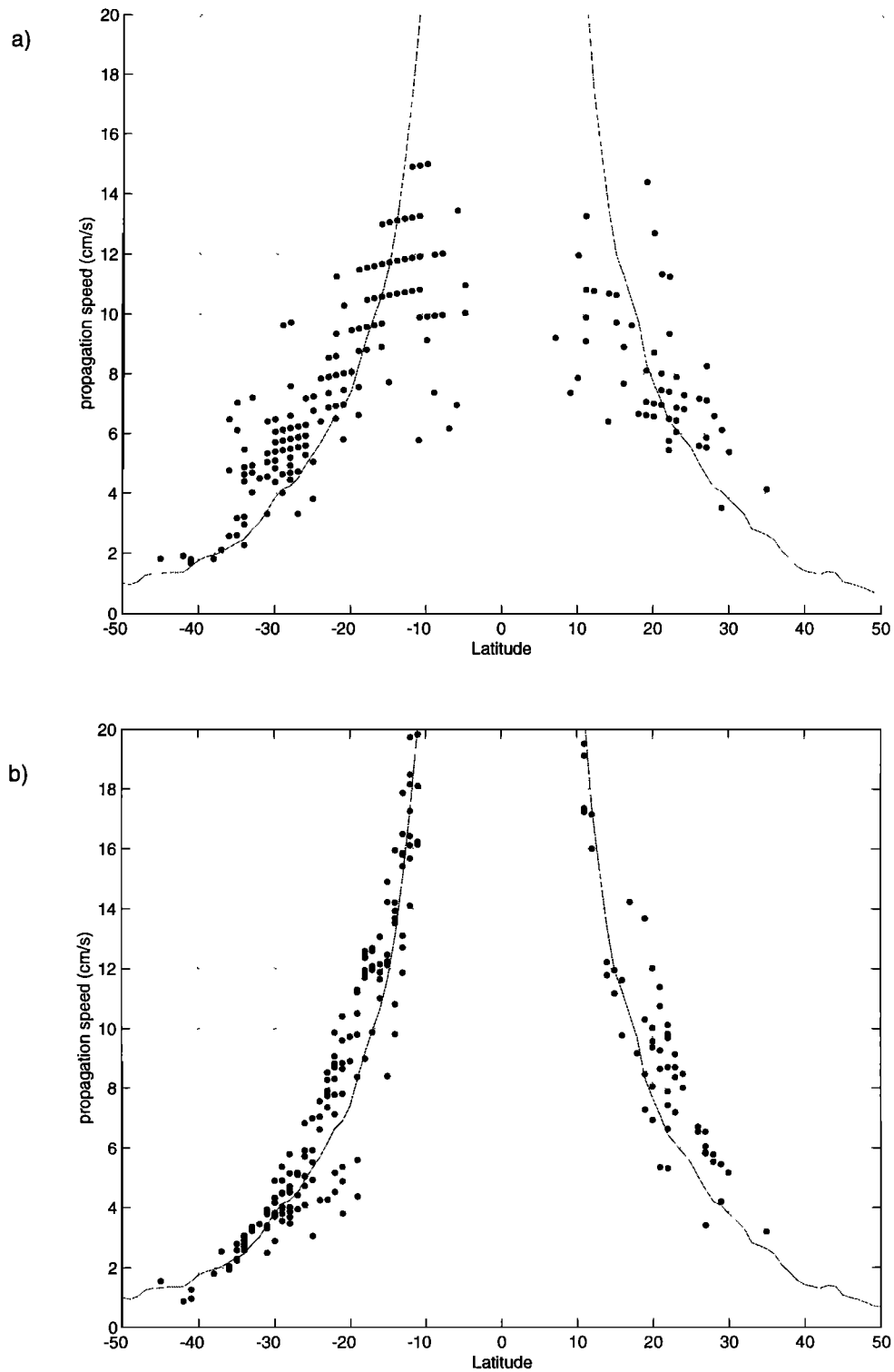


Figure 8. Plot of speed versus latitude showing (a) speed at each longitude where waves were detected from the Radon transform of the ASST record using a peak-to-average standard deviation ratio threshold of 2.3 and (b) *Killworth et al.*'s [1997] prediction of speed at the same locations as identified in Figure 8a. In both cases the solid line represents the zonal average of theoretical predictions for all longitudes at that latitude.

are strongly influenced by the Mid-Atlantic Ridge, consistent with our observations. *Wang and Koblinsky* [1994] used a simple model of barotropic and baroclinic Rossby wave behavior at ridges (two-layer with stepwise topography) to demonstrate that energy exchange occurs between the

baroclinic and barotropic modes at mid-ocean ridges. Depending on the ridge width and height, either mid-ocean generation of waves, dissipation of incident waves, or both can exist. These influences can be found in the ASST data set. For example, 20° and 27°S (Figures 10b and 10a) exhibit clear

examples of mid-ocean generation in the Pacific. When compared to the bathymetric transect for these latitudes, we observe that the generation of baroclinic waves seems to be related to broad bathymetric ridges, having a shallow slope. Conversely, in the Indian Ocean at 27°S, evidence of dissipation of the baroclinic energy is clear at the Madagascar Ridge. This behavior occurs when the ridge is narrow and steeply sloped.

These observations confirm the usefulness of the ASST data set for investigating topographic effects on Rossby wave propagation and point to the need for further data analysis coupled to theoretical modeling. For example, surveying the data systematically in order to identify the conditions (ridge height, width, slope and orientation, wave frequency, and wavenumber) for wave generation, dissipation, or change of speed is useful. Because the topography is likely to induce interactions between several baroclinic modes, clarifying how the surface thermal signature varies for the different modes will be important. The ASST data should be seen as a complement to global altimetry data for the study of Rossby wave interactions with bathymetry. The finer longitudinal resolution achieved by the ASST offers a clear benefit and is set to improve when 10 arc minute data become available.

7.4. Variation With Time

Although a thorough analysis of the wave speed variation over time is still to be performed, the SST-longitude-time plots themselves show some evidence that the propagation characteristics change. The most obvious temporal variability is seasonal. In Figures 2 and 3a, for example, in the eastern Pacific, annual discontinuities exist in the phase lines of the thermal wave signature. These occur in the local autumn and winter. The reappearance of the waves after a few months, with the phase structure almost aligned across the discontinuity, implies that the wave itself has continued to propagate. Its surface thermal signature has temporarily been lost, while the upper mixed layer temperature was dominated by other processes that have hidden the influence of the underlying dynamics.

Figure 3c is an example of where speed changes appear from year to year, most clearly evident at 45°E. This could be a result of changes in the underlying ocean structure, but another explanation is that different wave modes are apparent in different years, perhaps because the forcing is slightly different. Nonetheless, the consequence of thermal anomalies being propagated at different speeds in different years may be

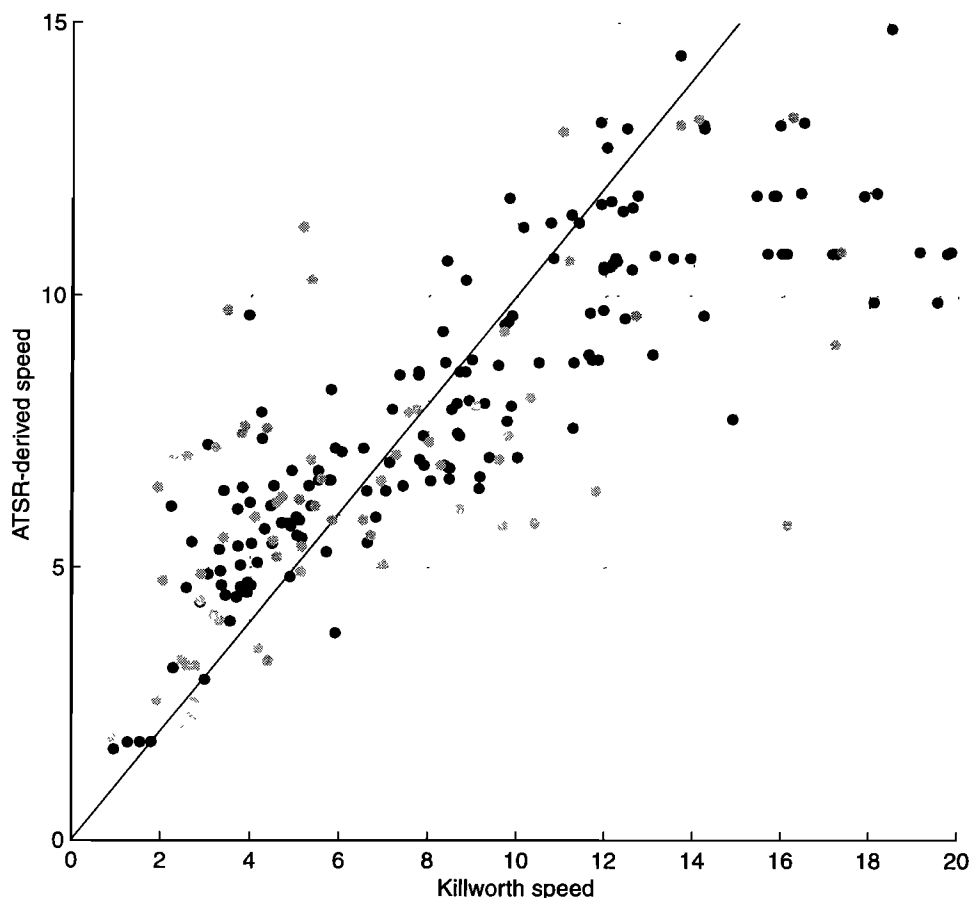


Figure 9. Scatterplot of Killworth *et al.* [1997] versus SST-detected speeds at each location where a strong thermal signature was detected. Solid dots are for peak-to-average standard deviation ratio > 2.4 , and shaded dots are for $2.3 < \text{ratio} < 2.4$.

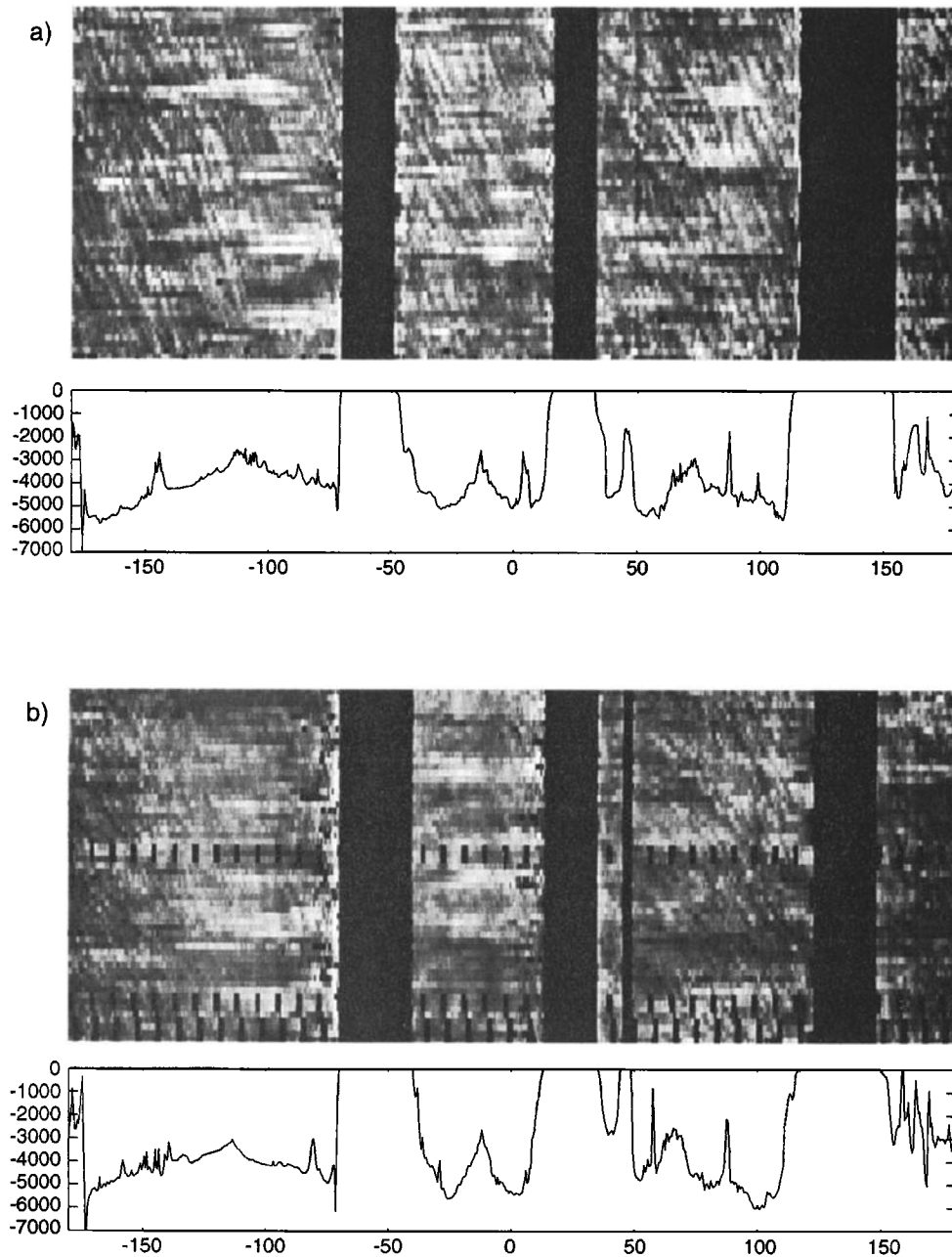


Figure 10. (a) Longitude-time plot of ASST-GOSTA anomaly at 27°S with bathymetry transect, and (b) longitude-time plot of ASST-GOSTA anomaly at 20°S with bathymetry transect.

important if they play a role in air-sea interaction feedback. Work is presently underway to examine the full ASST and ASST-2 (from ATSR-2) record and the longer AVHRR anomalies time series for evidence of systematic changes of speed that can be linked to short-period climate processes such as ENSO.

7.5. Eastward Propagating Features

Eastward propagating features can be seen in a number of locations in the Southern Ocean, for instance at 40° (Figure 6a) and at 48°S (Figure 6b). However, these features, whose speed ranges from 1 to 5 cm s⁻¹ eastward, are by no means ubiquitous in the ASST-GOSTA anomaly data set, as shown in

Plate 4. This is somewhat in contrast with their widespread distribution in the Antarctic Circumpolar Current observed by Hughes [1995] and Hughes *et al.* [1998] from model, SST, and altimeter data. In a zonal band between 40° and 45°S we occasionally observe fast (~20 cm s⁻¹) eastward propagating features whose nature remains unexplained, perhaps a residual annual signal.

The region where the eastward propagating Rossby waves are most evident in our data set (and where our results are most consistent with the previous observations) is the Indian sector of the Southern Ocean. The signatures observed there reflect the meandering nature and the velocity variations of the Antarctic Circumpolar Current. For instance, in Figure 6b,

Rossby wave features vary from nearly vertical "standing waves" (around 0°-10°E and 70°E) to gradually increasing eastward propagation. This reflects an increasing influence of the circumpolar current, as explained by Hughes [1996] and Hughes *et al.* [1998]. Baroclinic Rossby waves have a maximum phase and group speed relative to the mean flow, so when the flow becomes supercritical with respect to the waves, no wave can propagate westward. The signature of the eastward propagating features can then be used both to trace the current itself, as done by Hughes *et al.* [1998], and to study the spatial and temporal variations in its meandering.

An interesting side effect is that in supercritical conditions the current can extend deep enough to interact with the bottom topography, and this, in turn, means that the topography can play an important role in establishing the propagation characteristics of the waves themselves. All the above considerations call for further studies in this area, in particular to assess the effect of the southeastern and southwestern Indian Ridges on the waves.

8. Conclusions

This paper has identified the ubiquity, in finely resolved global SST records, of thermal signatures of planetary waves having Rossby wave-like propagation trajectories in longitude and time. Although the phenomenon has been detected previously, the evidence for its widespread occurrence at many latitudes and within all oceans has not previously been presented. Our initial objective in developing the analytical tools to determine the wave speed from the Hovmöller plots was to test Killworth *et al.*'s [1997] modifications to Rossby wave theory. A sufficient similarity exists between our observations of the longitude and latitude variations of propagation speed and the theory to confirm the initial assumption that many of the observed features are indeed the product of Rossby waves. At latitudes >20°, evidence of a small underestimate of the actual speed by Rossby wave theory, even as modified by Killworth *et al.* [1997], has been found. Also valuable information about Rossby wave propagation dependence on ocean bathymetry has been found. At latitudes <20° the temporal resolution of the data and uncertainty about which mode is being detected prevent us from concluding whether the slower than predicted wave speed observations are an artefact of the observing method or a real shortcoming of the theory.

In order to be able to use the thermal signatures to cast more light on the theory of Rossby wave propagation, we recommend further research in three directions. First, the theoretical models of Rossby wave propagation need to be adapted in order to represent their thermal signature explicitly, so that observations can be compared directly with theory. A further analysis of the possible role of atmospheric feedback on the propagation of the thermal anomalies is also desirable.

Second, scope for exploiting the available SST data sets more thoroughly exists. Work is under way by the authors to explore systematically the variations of propagation speeds over time. We intend to reduce the sampling window limitations by using the 10 arc minute resolution cells offered by the ASST-reanalyzed product and by averaging over a shorter time period. Use can also be made of the 3-4 day SST anomaly maps derived from AVHRR to explore faster waves at equatorial latitudes.

Third the analytical techniques can be improved further. Scope exists for developing the Radon transform analysis in

order to differentiate more clearly between peaks corresponding to propagating planetary waves and those associated with other phenomena. We will also attempt to apply a three-dimensional extension of the Radon transform analysis (P. G. Challenor, P. Cipollini, and D. Cromwell, Use of the Radon transform to examine the properties of oceanic Rossby waves, submitted to *Journal of Atmospheric and Oceanic Technology*, 2000) in order to identify whether Rossby waves with thermal signatures propagate with a nonzero meridional component. By focusing so far on measuring the characteristic speeds directly, we have not yet attempted to measure the wavenumber and frequency of the thermal waves. This is needed to help resolve the problem of mode ambiguity. It is also a prerequisite for exploring the origin of the waves, for example, whether they are atmospherically forced or arise as instabilities in the background mean flow. Application of standard two-dimensional spectral analysis to all but the strongest signatures is problematic because of the need to isolate the propagating features from the thermal signatures of other phenomena or just random SST fluctuations. Knowing the orientation of the constant phase lines from the method presented here will make it easier to apply a one-dimensional analysis to recover the time and length scales.

What has emerged from the analysis is that the global SST record contains a wealth of information about the westward (and in special cases the eastward) propagation of those planetary wave modes that have the strongest thermal signatures. These have an importance in their own right as well as provide a remotely sensed surface signature of a subsurface dynamical process that is otherwise difficult to observe. We believe our observations are potentially of wide interest to those studying air-sea interaction processes on the basin scale. There is a need to consider what impact these waves can have on the evolution of regional climate patterns. If they do play a significant role, then assimilating the measured speeds directly into climate models and forecasts should be possible in the future. Finally, we plan to examine the thermal signatures of the Rossby waves over as long a period as the records allow (more than 15 years in the case of the AVHRR data) to establish whether their propagation characteristics are correlated at all with established variability signals such as ENSO and the strength of monsoons.

References

- Barnier, B., A numerical study of the influence of the Mid-Atlantic Ridge on non-linear barotropic and first mode baroclinic Rossby waves generated by seasonal winds, *J. Phys. Oceanogr.*, 12, 417-433, 1988.
- Barton, I. J., A. J. Prata, and R. P. Cechet, Validation of the ATSR in Australian waters, *J. Atmos. Oceanic Technol.*, 12, 290-300, 1995.
- Bottomley, M., C. K. Folland, J. Hsiung, R. E. Newell, and D. E. Parker, Global ocean surface temperature atlas: Joint project, 20 pp., Her Majesty's Stn. Off., Norwich, England, U.K., 1990.
- Chelton, D. B., and M. G. Schlax, Global observations of oceanic Rossby waves, *Science*, 272, 234-238, 1996.
- Chelton, D. B., R. A. deSzoeke, M. G. Schlax, K. El Naggar, and N. Siwertz, Geographical variability of the first baroclinic Rossby radius of deformation, *J. Phys. Oceanogr.*, 28, 433-460, 1998.
- Cipollini, P., D. Cromwell, and G. D. Quartly, Variability of Rossby wave propagation in the North Atlantic from TOPEX/Poseidon altimetry, paper presented at International Geoscience and Remote Sensing Symposium, The Institute of Electrical and Electronics Engineers, Lincoln, Nebraska, 27-31 May, 1996.
- Cipollini, P., D. Cromwell, M. S. Jones, G. D. Quartly, and P. G. Challenor, Concurrent altimeter and infra-red observations of

- Rosby wave propagation near 34°N in the northeast Atlantic, *Geophys. Res. Lett.*, *24*, 889-892, 1997.
- Deans, S. R., *The Radon Transform and Some of Its Applications*, John Wiley, New York, 1983
- Dickinson, R. E., Rossby waves: Long period oscillations of oceans and atmospheres, *Annu. Rev. Fluid Mech.*, *10*, 159-195, 1978.
- Donlon, C. J., and I. S. Robinson, Radiometric validation of ERS-1 along track scanning radiometer average sea surface temperature in the Atlantic Ocean, *J. Atmos. Oceanic Technol.*, *15*, 647-660, 1998.
- Edwards, T., et al., The along-track scanning radiometer: Measurement of sea surface temperature from ERS-1, *J. Br. Interplanet. Soc.*, *43*, 160-180, 1990.
- Emery, W. J., and L. Magaard, Baroclinic Rossby waves as inferred from temperature fluctuations in the eastern Pacific, *J. Mar. Res.*, *34*, 365-385, 1976.
- Emery, W. J., W. G. Lee, and L. Magaard, Geographic and seasonal distribution of Brunt-Väisälä frequency and Rossby radii in the North Pacific and North Atlantic, *J. Phys. Oceanogr.*, *14*, 294-317, 1984.
- Gerdes, R., and C. Wübbler, Seasonal variability in the North Atlantic Ocean: A model intercomparison, *J. Phys. Oceanogr.*, *21*, 1300-1322, 1991.
- Gill, A. E., *Atmosphere-Ocean Dynamics*, 662 pp., Academic, San Diego, Calif., 1982.
- Graham, N. E., and W. B. White, The El Niño cycle, a natural oscillator of the Pacific ocean-atmosphere system, *Science*, *240*, 1293-1302, 1988.
- Graham, N., and W. B. White, The role of the western boundary in the ENSO cycle: Experiments with coupled models, *J. Phys. Oceanogr.*, *20*, 1935-1948, 1990.
- Halliwell, G. R., P. Cornillon, and D. A. Byrne, Westward-propagating SST anomaly features in the Sargasso Sea, 1982-1988, *J. Phys. Oceanogr.*, *21*, 635-639, 1991a.
- Halliwell, G. R., Y. J. Ro, and P. Cornillon, Westward-propagating SST anomalies and baroclinic eddies in the Sargasso Sea, *J. Phys. Oceanogr.*, *21*, 1664-1680, 1991b.
- Herrmann, P., and W. Krauß, Generation and propagation of Annual Rossby waves in the North Atlantic, *J. Phys. Oceanogr.*, *19*, 727-744, 1989.
- Houry, S., E. Dombrowsky, P. De Mey, and J.-F. Minster, Brunt-Väisälä and Rossby radii in the South Atlantic, *J. Phys. Oceanogr.*, *17*, 1619-1626, 1987.
- Hughes, C. W., Rossby waves in the Southern Ocean: A comparison of TOPEX/Poseidon altimetry with model predictions, *J. Geophys. Res.*, *100*, 15,933-15,950, 1995.
- Hughes, C. W., The Antarctic Circumpolar Current as a waveguide for Rossby waves, *J. Phys. Oceanogr.*, *26*, 1375-1387, 1996.
- Hughes, C. W., M. S. Jones, and S. Charnochan, Use of transient features to identify eastward currents in the Southern Ocean, *J. Geophys. Res.*, *103*, 2929-2943, 1998.
- Jacobs, G. A., W. J. Emery, and G. H. Born, Rossby waves in the Pacific Ocean extracted from Geosat altimetry data, *J. Phys. Oceanogr.*, *23*, 1155-1175, 1993.
- Jacobs, G. A., H. E. Hurlburt, J. C. Kindle, E. J. Metzger, J. L. Mitchell, W. J. Teague, and A. J. Wallcraft, Decade-scale trans-Pacific propagation and warming effects of an El Niño anomaly, *Nature*, *370*, 360-363, 1994.
- Jones, M. S., M. A. Saunders, and T. H. Guymer, Reducing cloud contamination in ATSR averaged sea surface temperature data, *J. Atmos. Oceanic Technol.*, *13*, 492-506, 1996a.
- Jones, M. S., M. A. Saunders, and T. H. Guymer, Global remnant cloud contamination in the along-track scanning radiometer data: Source and removal, *J. Geophys. Res.*, *101*, 12,141 - 12,147, 1996b.
- Kang, Y. Q., and L. Magaard, Annual baroclinic Rossby waves in the central North Pacific, *J. Phys. Oceanogr.*, *10*, 1159-1167, 1980.
- Kessler, W. S., Observations of long Rossby waves in the northern tropical Pacific, *J. Geophys. Res.*, *95*, 5183-5217, 1990.
- Kessler, W. S., Can reflected extra-equatorial Rossby waves drive ENSO?, *J. Phys. Oceanogr.*, *21*, 444-452, 1991.
- Killworth, P. D., and J. R. Blundell, The effect of bottom topography on the speed of long extratropical planetary waves, *J. Phys. Oceanogr.*, *29*, 2689-2710, 1999.
- Killworth, P. D., D. B. Chelton, and R. A. de Szoeke, The speed of observed and theoretical long extratropical planetary waves, *J. Phys. Oceanogr.*, *27*, 1946-1966, 1997.
- Kirtman, B. P., Oceanic Rossby wave dynamics and the ENSO period in a coupled model, *J. Climate*, *10*, 1690-1704, 1997.
- LeBlond, P. H., and L. A. Mysak, *Waves in the Ocean*, 602 pp., Elsevier Sci., New York, 1978.
- Le Traon, P.-Y., and P. De Mey, The eddy field associated with the Azores front east of the mid-Atlantic Ridge as observed by the Geosat altimeter, *J. Geophys. Res.*, *99*, 9907-9923, 1994.
- Meyers, G., On the annual Rossby wave in the tropical North Pacific Ocean, *J. Phys. Oceanogr.*, *9*, 663-674, 1979.
- Murray, M. J., *Sea Surface Temperatures From ATSR (August 1991 to July 1995)* [CD-ROM], Rutherford Appleton Lab., Chilton, England, U.K., 1995.
- Murray, M. J., M. R. Allen, C. T. Mutlow, A. M. Závody, M. S. Jones, and T. N. Forrester, Actual and potential information in dual-view radiometric observations of sea surface temperature from ATSR, *J. Geophys. Res.*, *103*, 8153-8165, 1998.
- Mutlow, C. T., A. M. Závody, I. J. Barton, and D. T. Llewellyn-Jones, Sea surface temperature measurements by the along-track scanning radiometer on the ERS-1 satellite: Early results, *J. Geophys. Res.*, *99*, 575-588, 1994.
- Picaut, J., and L. Sombardier, Influence of density stratification and bottom depth on vertical mode structure functions in the tropical Pacific, *J. Geophys. Res.*, *98*, 14,727-14,737, 1993.
- Polito, P. S., and P. Cornillon, Long baroclinic Rossby waves detected by TOPEX/Poseidon, *J. Geophys. Res.*, *102*, 3215-3235, 1997.
- Radon, J., Über die Bestimmung von Funktionen durch ihre Integralwerte längs gewisser Mannigfaltigkeiten, *Ber. Sächsische Akad. der Wissenschaften*, *69*, 262-267, 1917. (English translation, S. R. Deans, *The Radon Transform and Some of Its Applications*, pp. 204-217, John Wiley, New York, 1983.)
- Rosby, C.-G., Planetary flow patterns in the atmosphere. *Q. J. R. Meteorol. Soc.*, *66*, suppl., 68-97, 1939.
- Tokmakian, R. T., and P. G. Challenor, Observations in the Canary Basin and the Azores Frontal Region using Geosat data, *J. Geophys. Res.*, *98*, 4761-4773, 1993.
- Van Woert, M. L., and J. M. Price, Geosat and advanced very high resolution radiometer observations of oceanic planetary waves adjacent to the Hawaiian Islands, *J. Geophys. Res.*, *98*, 14,619-14,631, 1993.
- Wang, L., and C. J. Koblynski, Influence of mid-ocean ridges on Rossby waves, *J. Geophys. Res.*, *99*, 25,143-25,153, 1994.
- White, W. B., Annual forcing of baroclinic long waves in the tropical North Pacific Ocean, *J. Phys. Oceanogr.*, *7*, 51-61, 1977.
- White, W. B., The resonant response of interannual baroclinic Rossby waves to wind forcing in the eastern and mid-latitude North Pacific, *J. Phys. Oceanogr.*, *15*, 403-415, 1985.
- White, W. B., and J. F. T. Saur, A source of annual baroclinic waves in the eastern subtropical North Pacific, *J. Phys. Oceanogr.*, *11*, 1452-1462, 1981.
- White, W. B., and J. F. T. Saur, Sources of interannual baroclinic waves in the eastern subtropical North Pacific, *J. Phys. Oceanogr.*, *13*, 531-544, 1983.
- White, W. B., and C.-K. Tai, Reflection of interannual Rossby waves at the western boundary of the tropical Pacific, *J. Geophys. Res.*, *97*, 14,305-14,322, 1992.
- White, W. B., C.-K. Tai, and J. Dimento, Annual Rossby wave characteristics in the California Current region from the Geosat exact repeat mission, *J. Phys. Oceanogr.*, *20*, 1297-1311, 1990a.
- White, W. B., N. Graham, and C.-K. Tai, Reflection of annual Rossby waves at the maritime western boundary of the tropical Pacific, *J. Geophys. Res.*, *95*, 3101-3109, 1990b.
- White, W. B., Y. Chao, and C.-K. Tai, Coupling of biennial oceanic Rossby waves with the overlying atmosphere in the Pacific Basin, *J. Phys. Oceanogr.*, *28*, 1236-1251, 1998.
- Zavody, A. M., M. R. Gorman, D. J. Lee, D. Eccles, C. T. Mutlow, and D. T. Llewellyn-Jones, The ATSR data processing scheme developed for the EODC, *Int. J. Remote Sens.*, *15*, 827-843, 1994.
- Zavody, A. M., C. T. Mutlow, and D. T. Llewellyn-Jones, A radiative transfer model for SST retrieval for the ATSR, *J. Geophys. Res.*, *100*, 937-952, 1995.

P. Cipollini, James Rennell Division for Ocean Circulation and Climate, Southampton Oceanography Centre, Southampton SO14 3ZH, England, U.K. (cipo@soc.soton.ac.uk)

K. L. Hill and I. S. Robinson, School of Ocean and Earth Science, Southampton Oceanography Centre, European Way, Southampton, SO14 3ZH, England, U.K. (isr@soc.soton.ac.uk)

(Received May 20, 1999; revised December 22, 1999; accepted March 28, 2000)